JOURNAL OF MATERIALS SCIENCE 19 (1984) 3895–3907

Inherent ductility in amorphous Ta_2O_5 films

HANI RIZKALLA, STEPHEN T. WELLINGHOFF
Department of Chemical Engineering and Materials Science, University of Minnesota, 151 Amundson Hall, 421 Washington Avenue SE, Minneapolis, Minnesota 55455, USA

Thin films (30 to 80 nm) of refractory tantalum metal were successfully sputter-deposited on uniformly deformable fluoropolymer and polyimide substrates in stress free form. These films were later anodized into amorphous Ta_2O_5 which is a non-porous (barrier-type) oxide with excellent corrosion resistant properties. X-ray photo-emission spectroscopy studies were carried out on tantalum and Ta_2O_5 to determine the chemical composition and oxidation states of elements. Thin tantalum and Ta_2O_5 films on fluoropolymer substrates contained fluorine as an impurity while similar films on polyimide substrate contained no fluorine and, in general, fewer impurities. Both thin tantalum films and the corresponding anodic oxides, when deformed in tension to 10% strain, exhibited the expected ductile behaviour of metals where slip bands were observed in the electron microscope. In some cases, minor cracks were observed in the deformed anodic films due to suspected local detachment of the film from the substrate.

1. Introduction

There is a growing interest in producing thin oxide films which will act as protective barriers against corrosion. The degree of protection achieved by these coatings depends on both the chemical and mechanical properties of the film. More specifically, the adhesion between the coating and the substrate as well as the ability of the coating to deform extensively and relieve stresses without cracking or peeling is of prime importance. Anodic films grown on either single or polycrystalline metallic substrates have been looked at most extensively. These thin oxide films showed a degree of ductility under some conditions. However, both the reported values for strain at failure and mode of failure differ considerably from one investigation to another. The fracture morphology and the value of strain at failure for Al_2O_3 depend on the anodization voltage and on the film thickness [1]. Anodic films grown at voltage less than 30 V fracture along substrate slip steps at a failure strain of $\simeq 1.1\%$ provided that the thickness is less than 40 nm. Adherent Al_2O_3 of this type can often extend the elastic range of the substrate by suppressing surface dislocation generation [2–6]. Porous Al_2O_3 films, grown at 30 V or higher fracture normal to tensile axis at a failure strain of $\simeq 0.9\%$ [1, 7]. Porous oxide of poor adherence, however, fractures at much lower strains (0.1 to 0.3%) [8, 9].

A similar range of results has been obtained for anodic Ta_2O_5 coatings. Bubar and Vermilyea [10] used an electrochemical method to measure the amount of bare tantalum metal exposed by cracking of an anodic Ta_2O_5 coating during straining of a tantalum wire. Amazingly, the adherent oxide deformed plastically with no cracking out to 50% elongation. In contrast, low fracture strains ($\simeq 0.81\%$) were obtained in a dry bulge test after selectively removing known areas of the metallic substrate [11]. Optical and transmission electron microscopy revealed that anodic films grown on mechanically polished tantalum failed at $\simeq 0.28\%$ strain regardless of the thickness, while films grown on chemically polished tantalum failed at $\simeq 0.2\%$ at thicknesses less than 68 nm and $\simeq 0.14\%$ strain for thicker films (Choo and Devereux [1]). However, in a relatively recent paper, Propp and Young [12] emphasized that some pre-treatment is necessary for chemically polished substrates prior to anodization in order to form adherent coatings. Immersion for a few minutes in boiling water is apparently required to remove the fluoride film left by chemical polishing [13]. When these

0022–2461/84 $03.00 + .12

precautions were taken, anodic Ta_2O_5 oxide films on tantalum substrates were observed to undergo a thickness reduction up to 6% in tensile deformation, and up to 15% reduction during rolling perpendicular to the oxide thickness direction [12]. In a related piece of work, Sethi and Gibala [14–17] reported that an anodic Nb_2O_5 or Ta_2O_5 film increases the critical resolved shear stress of niobium and tantalum metal, respectively, at room temperature. At lower temperatures, softening occurs. According to these authors, the presence of an oxide film inhibits slip step emergence at the surface of single crystal metallic substrates at room temperature, while at lower temperatures, the oxide–metal interface acts as a source of mobile dislocations. Electron microscope investigations revealed that dislocation steps, emerging from the metal, plastically deformed the oxide coating, leaving it adherent and uncracked.

The purpose of the present work is to define the inherent ductility of thin amorphous Ta_2O_5 films in the absence of an underlying tantalum substrate to avoid the complicating effects of localized deformation and interfacial stresses. Our intetest in the mechanical properties of anodic Ta_2O_5 films has its source in their superior chemical resistance even in hostile wet chlorine environments [18]. This property, when coupled with good ductility, should provide for an impenetrable barrier film with very good interfacial crack resistance. These properties should be compared to plasma polymerized organics which can act as barriers to small molecules at high cross-link densities but consequently lose ductility [19].

2. Experimental procedures

Thin films of tantalum were first sputter-deposited on uniformly deformable fluropolymer (FEP-Type A, 12.7×10^{-2} mm thick) and polyimide (Kapton-Type V, 7.62×10^{-2} mm thick) film substrates (Du Pont de Nemours & Co.). Both β-tantalum and b c c-tantalum films of different morphology were obtained by varying the residual gas pressure, i.e., impurity content prior to deposition [20]. The final quality of the deposited film depends on the argon gas pressure, target to substrate distance, pre-sputtering time, applied forward power and the chemical nature of the substrate [21–26]. Tantalum film thicknesses were measured by α step on glass slides placed adjacent to the polymer substrate and partially covered during metal deposition. However, the α step method did not yield accurate results below 70 nm. For thinner films a reflective gold layer was deposited across the tantalum film edge on the glass slide. Interference microscopy was used to observe the fringe pattern shift that occurred across the tantalum film edge. The film thickness, t, is given by

$$t = \frac{\Delta L}{L} \times \frac{\lambda}{2},$$

where ΔL is the displacement of the fringes, L is the fringe spacing and λ is the wavelength of the monochromatic light source [27].

Some of the tantalum films were prepared for anodization on the plastic substrate by first degreasing with acetone, washing with distilled water, drying and then applying electrical contacts with silver paste and thin copper wires. The anodization was carried out in a water solution of 0.01 wt% citric acid (pH 2.7) first at constant current density of 0.2 mA cm^{-2} until a pre-determined voltage value was reached. Then, films were held at constant voltage for 30 min whereupon the current decayed rapidly, completing the anodization process and producing transparent films of typically golden colour. The chemical composition of both tantalum metal and anodized films was determined by X-ray photo-emission spectroscopy (XPS) (Physical Electronics 555). The photoelectron binding energies were normalized to the carbon 1*s* contaminant present on all samples. Argon ion sputtering was used to identify the relative concentration and oxidation state of elements at 1 to 1.5 nm thickness intervals from the surface of the deposited film to the substrate interface.

All β- and b c c-tantalum films as well as anodized films were mechanically deformed on the polymer substrates to 5% and 10% tensile strain at a strain rate of 5% min^{-1}. A 10 nm thick brittle carbon film was evaporated onto the deformed film so that any deformation during subsequent handling of the deformed film could be observed as a crack in the carbon layer during transmission microscopy observation. All samples were then coated with a polyacrylic acid solution which was allowed to evaporate to a hard adherent film. After stripping the film from the substrate the polyacrylic acid was dissolved in water and the floating tantalum and Ta_2O_5 films taken up on a microscope grid to be examined in the scanning transmission electron microscope (STEM JEOL 100-C). In addition, carbon–platinum replacas

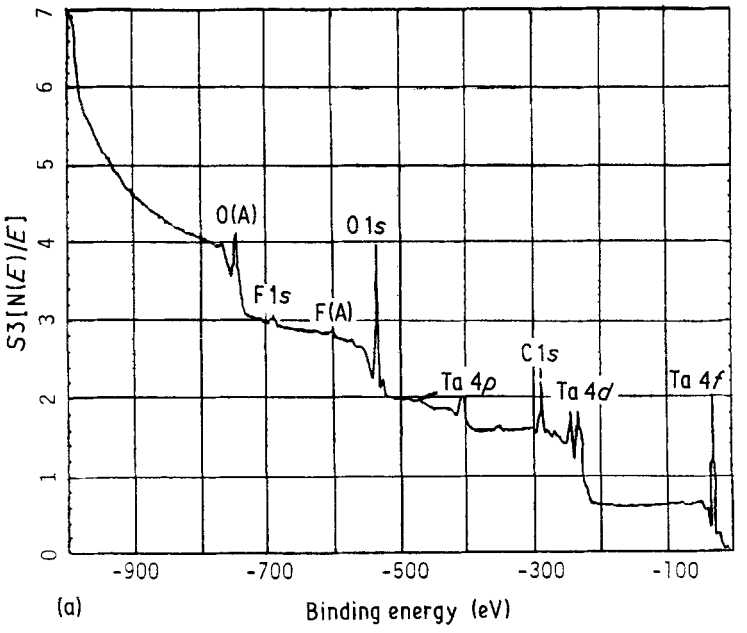

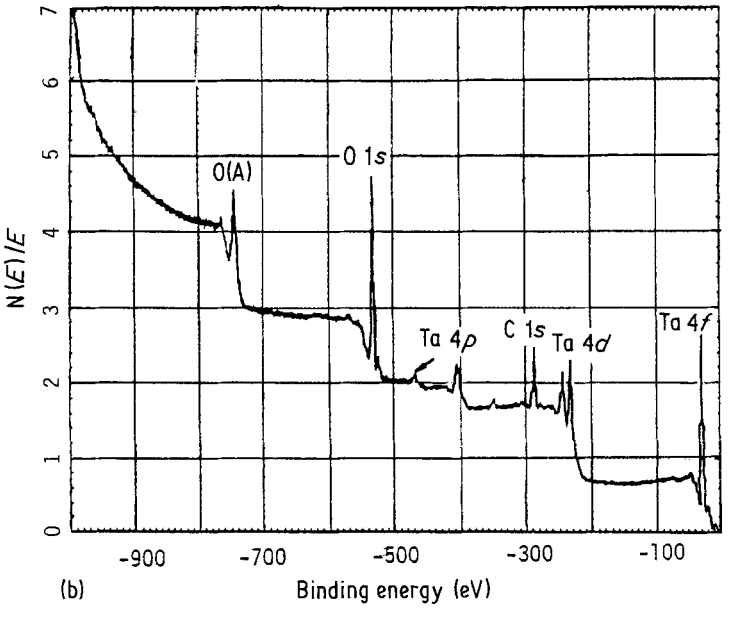

Figure 1 (a) A typical XPS survey on the surface of anodic Ta_2O_5 on FEP substrate. (b) Similar to (a), but the substrate is Kapton. Note the disappearance of the fluorine peaks.

of the polymer substrate were prepared and examined in the STEM. Examination of this replica made it possible to distinguish between actual deformation morphology in the thin films and substrate processing traces.

3. Results

3.1. Chemical composition

The initial XPS survey showed that all tantalum and Ta_2O_5 films (on FEP substrates) contained the following elements: oxygen, carbon, fluorine and tantalum (Figs. 1a, b). Similar results were obtained for sputter-deposited tantalum films on polyimide (Kapton) substrate except that fluorine was not detected. The presence of nitrogen, due to the Kapton substrate, was difficult to detect by XPS because the nitrogen 1*s* peak overlapped the strong tantalum $4p_{3/2}$ peak. Therefore, an Auger analysis was carried out in order to investigate the nature and concentration of nitrogen present in the thin films. A $4f_{5/2}$, $4f_{7/2}$ doublet characteristic of Ta^{+5} appeared on the surface of all sputtered tantalum films. This thin thermal oxide layer disappeared after three minutes of

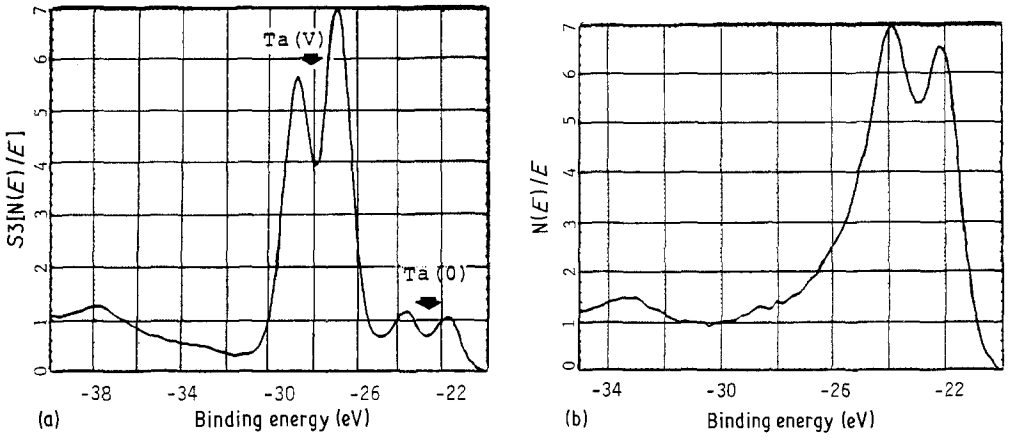

Figure 2 (a) Graph showing the presence of thin oxide layer (Ta_2O_5) on the surface of tantalum films. (b) The Ta^{+5} peak disappeared after 3 min etching with argon ions.

sputter etching with argon ions (the rate of etching was ~ 1.4 nm min^{-1}, suggesting that the maximum thickness of this thermal oxide layer was ~ 4 nm) (Figs. 2a, b).

3.1.1. 1s oxygen peak

An oxygen peak was detected in all samples of tantalum and Ta_2O_5 regardless of the substrate (FEP or Kapton) and the phase of the deposited tantalum (β or b c c). In general, the 1*s* oxygen peak appeared to be symmetrical at 531.6 eV, with a small overlapping shoulder at a 2.0 eV higher energy. The source of this shoulder was suspected to be chemisorbed hydroxyl (OH) group or water vapour. A multiplex for the oxygen peak in a sample of Ta_2O_5/Kapton was carried out before and after heating for 2 h. at 150° C, but the small shoulder remained detectable but less intense, suggesting that the presence of chemisorbed oxygen noticeably affects the Ta/O ratio (Fig. 3). Elimination of bound water or chemisorbed oxygen requires heating to temperatures of 400 to 500° C, which was impossible to obtain with the polymeric substrate.

As mentioned before, the oxygen was detected in both metallic and anodic films. For metallic films (mixture of β and b c c phases), the Ta/O ratio (1/0.3) was relatively high within the first 15 to

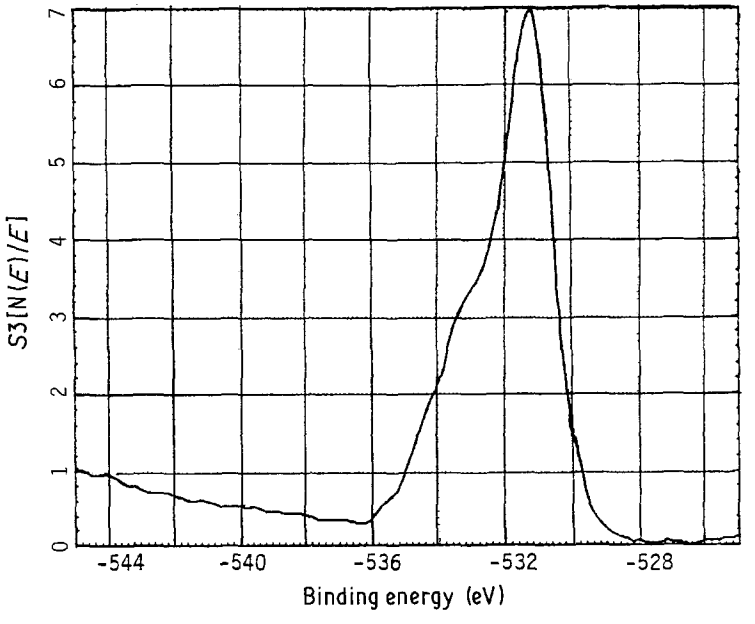

Figure 3 A symmetrical oxygen peak at 531.6 eV with an overlapping shoulder at slightly higher binding energy (≃ 1.6 eV higher) This shoulder could be due to chemisorbed OH groups.

TABLE Ia Tantalum films on FEP substrate

Etching time (min)	C (at%)	F (at%)	Ta (at%)	O (at%)	Ta/O
0	53.5	–	12.5	34.0	1/2.72
3	39.6	8.7	46.6	5.2	1/0.1
6	22.1	11.0	50.8	16.1	1/0.3
8	18.8	17.2	47.4	16.6	1/0.35
22	28.2	22.3	46.9	2.5	1/0.05

20 nm of the surface due to thermal oxidation and chemisorbed oxygen. However, the bulk of the film was metallic in nature with Ta/O as low as 1/0.05 (Table Ia). Similar behaviour was observed in the case of anodic oxide films from b c c- and β-tantalum films, where excess oxygen was detected on the surface (Ta/O was 1/3.9 and 1/3.7, respectively). The Ta/O ratio decreases continuously as the metal–substrate interface is approached, as expected from the diffusion limitations of oxygen in thick coherent oxide films (Tables Ib and Ic). An XPS analysis on standard crystalline Ta_2O_5 powder (Alfa products) is shown in Table Id. More than 40 nm of surface must be removed, before the correct stoichiometry is obtained.

Excluding the surface layer, the Ta/O ratio in the bulk of the oxide was in the range between 1/2.4 to 1/2.0, indicating a mixture of Ta_2O_5 and the TaO_2. In addition, anodic films grown from b c c- and β-tantalum films had almost the same chemical composition except that films grown from b c c-tantalum had a slightly higher oxygen solubility (refer to Tables Ib and Ic). Generally, the deviation from stoichiometry could be accounted for by the following errors: (i) errors in sensitivity factors and estimation of the area under the peaks; (ii) physically and/or chemically absorbed excess oxygen trapped inside the films during sputtering or anodization.

3.1.2. Tantalum peak

The characteristic $4f_{5/2}$, $4f_{7/2}$ doublet of tantalum-(0) appeared at binding energies of 21.7eV and 2.35 eV respectively (Fig. 2a). Upon anodic oxidation of tantalum(0) to tantalum(V), the chemical shift was so large that the entire tantalum $4f$ doublet moved to a 5 eV higher binding energy. Moreover, the tantalum(V) in both anodic Ta_2O_5 and the standard Ta_2O_5 was reduced to a lower oxidation state due to bombardment with argon ions during sputter etching in the XPS spectrophotometer (Fig. 4), which is a commonly observed phenomenon during profiling of oxides.

3.1.3. 1s carbon peak

Carbon is usually observed in XPS studies as unavoidable surface contamination from the atmosphere. The position of the carbon peak can also be used to calculate the amount of binding energy shift due to the charging effects in semiconducting and insulating materials. During the present work, an initial high carbon concentration was detected on the surface of both tantalum and Ta_2O_5 films. Surprisingly, the same high carbon concentration was observed on the standard Ta_2O_5 sample, suggesting that atmospheric carbon was a major source of contamination (refer to Tables Ia to Id). As the surface layer was etched away, the carbon concentrations kept decreasing within the bulk of the thin film (tantalum and

TABLE Ib Anodic Ta_2O_5/FEP (initially Ta has b c c phase)

Etching time (min)		C (at%)	F (at%)	Ta (at%)	O (at%)	Ta/O
Surface	0	35.7	0.1	13.1	51.2	1/3.9
	3	21.3	7.3	17.7	53.7	1/3.03
	6	18.9	7.8	17.3	56	1/3.24
	9	22.3	6.5	17.5	53.8	1/3.07
	12	24.5	6.1	17.2	52.2	1/3.03
	20	24.3	4.4	19	52.3	1/2.75
	30	24.4	5.1	19.7	50.8	1/2.57
Polymer Substrate						

TABLE Ic Anodic Ta_2O_5/FEP (initially Ta has β-phase)

Etching time (min)	C (at%)	F (at%)	Ta (at%)	O (at%)	Ta/O
0	64.1	1.9	7.1	26.8	1/3.77
6	59.0	3.0	8.0	30	1/3.75
15	19.0	9.4	23.4	48.2	1/2.05
24	2.8	12.9	27.9	56.5	1/2.03
33	11.5	9.2	29.6	51.6	1/1.87
Polymer Substrate					

Ta_2O_5). Upon getting close to the film–substrate interface (especially in the case of FEP substrate), the carbon concentration increased rapidly. The same behaviour was observed for films deposited on polyimide (Kapton) substrate, except that the carbon concentration within the bulk of the film was lower than that observed for films deposited on FEP substrates. In general, the carbon in the deposited films, regardless of the substrate, originated mainly from atmospheric carbon (for tantalum, Ta_2O_5), in smaller amounts, from organic electrolyte carbon (in case of Ta_2O_5), and finally, from carbon originating in the polymeric substrate.

A second carbon peak was frequently observed at ~ 282 eV, in tantalum and Ta_2O_5/FEP, suggesting hydrocarbon compounds. The secondary carbon peak observed at high binding energy (292 eV) undoubtedly represents flurocarbon compounds.

3.1.4. 1s fluorine peak

Fluorine was detected only in films deposited on FEP substrates in low concentration on the surface (1 to 9 at%) and in increasing amounts as the film–substrate interface was approached (20 to 50 at%). The FEP substrate was the only possible source for fluorine, which could have been knocked off as fluorocarbon and trapped inside the tantalum films during the sputter-deposition process when the polymer substrate was hit by energetic tantalum atoms.

TABLE Id Standard crystalline Ta_2O_5

Etching time (min)	C (at%)	Ta (at%)	O (at%)	Ta/O
0	47.9	10.9	41.2	1/3.78
5	50.7	10.7	38.7	1/3.62
10	46.7	43.2	40.2	1/3.05
15	47.7	14.2	38.2	1/2.69

3.1.5. Nitrogen peak

The Auger peak (KVV = 873.5 eV, and XPS BE for 1s = 39 eV) was detected only for films deposited on polyimide (Kapton) and had a very small concentration on the surface (0.7 at%) which kept increasing as the interface was approached (8% to 9%). As in the case of fluorine in FEP substrate, nitrogen could be knocked off and trapped as an organic fragment during deposition.

Generally, films deposited on Kapton substrates contained less contamination. The carbon concentration was less, no fluorine was detected, and nitrogen concentration was low within the bulk of the films.

3.2. Morphology and mechanical properties

In order to obtain high quality anodic films, the initial sputter-deposited tantalum films must adhere to the polymeric substrate and possess a minimum amount of internal stress due to the preparation method. Therefore, tantalum films sputter-deposited under a variety of sputtering conditions were examined with optical and scanning transmission electron microscopy (STEM). Films deposited under d.c. sputtering conditions at low voltage and high argon pressure yielded low density, porous tantalum films of high electrical resistivity. The porous β-tantalum film

TABLE Ie Anodic Ta_2O_5 on Kapton substrate

Etching time (min)	C (at%)	Ta (at%)	O (at%)	Ta/O
0	37.3	14.4	48.3	1/3.35
3	11.7	21.4	66.9	1/3.13
6	10.3	22.4	67.3	1/3.0
9	10.3	23.2	66.1	1/2.85
12	10.0	23.9	66.1	1/2.76
20	8.8	25.6	56.6	1/2.56
30	11.4	27.1	61.5	1/2.27

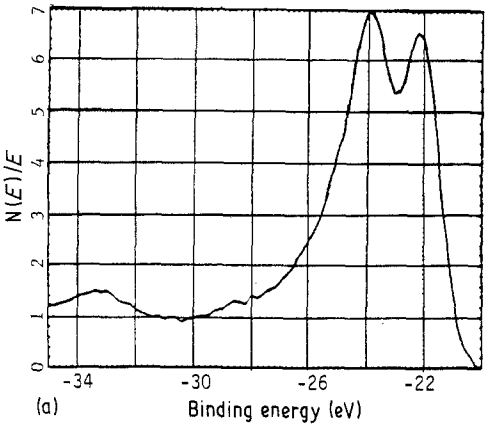

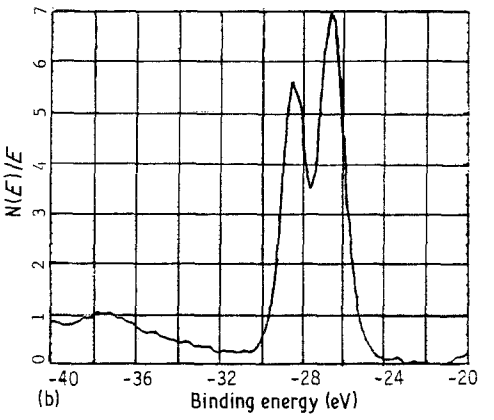

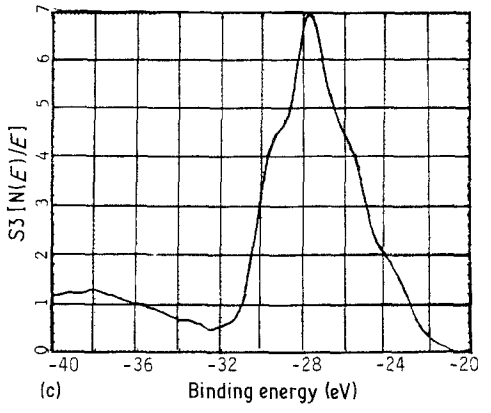

Figure 4 (a) A typical Ta(0) $f_{5/2}$, $f_{7/2}$ doublet which normally appears at 21.7 eV. In this figure the peak is slightly shifted due to charging. (b) The shift in the Ta(0) doublet upon anodic oxidation to Ta(V). (c) Tantalum is usually reduced due to argon ion bombardment.

readily absorbed oxygen, isolating metal grains in a matrix of insulating Ta_2O_5 [21, 22]. Reduced surface mobility of tantalum atoms during sputtering at high argon pressure might be responsible for this structure (Fig. 5a). To improve this situation, a series of tantalum films was deposited at different forward powers (200, 300 and 400 W) and moderate target bias (1.5 to 2.5 kV) using r.f. sputtering (Perkin Elmer 2400-85A) at an argon pressure of 8×10^{-3} torr. Unfortunately, as a consequence of heating by secondary electrons from the overlaying plasma and the low thermal conductivity of the polymer substrate, the films were grown at temperatures between 100 and 200° C. Since the tantalum film and the polymer substrate have large thermal expansion coefficient differ-

TABLE II

Element	Before etching		After etching	
	Binding energy (eV)	Expectations	Binding energy (eV)	Expectations
C	285	Carbon from electrolyte	285	Same
			282	$(CH_2)_n$
			292	Carbon attached to fluorine from substrate.
F	689	Fluorine covalently bonded to carbon in form of $(CF_2)_n$	689	Same as before with an added feature of fluorine covalently bonded to substrate carbon.
			685	Fluorine from substrate by diffusion.
O	531.6	O_2 due to anodization	531.6	Same.
Ta	26.7	Ta_2O_5	26.7	Ta_2O_5
	28.6	Ta_2O_5	29	Ta_2O_5
			23	Could be a lower oxidation state of Ta.

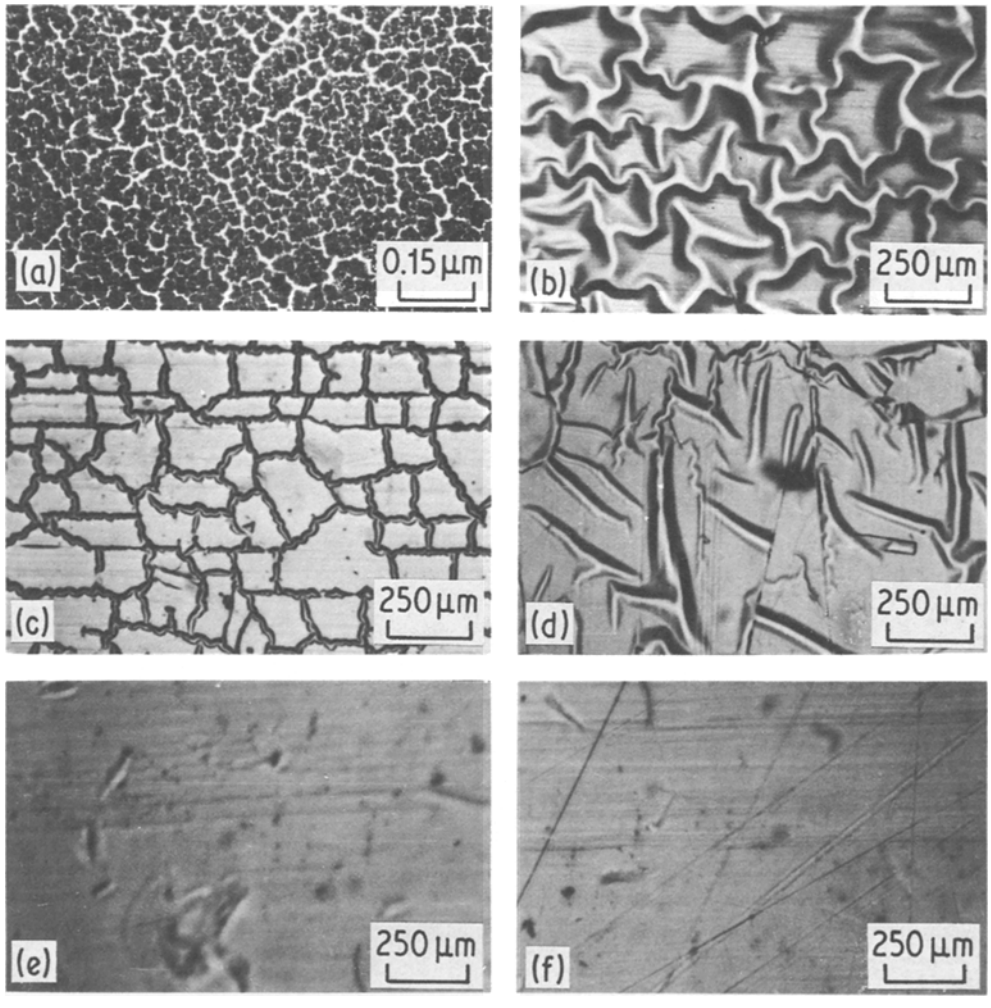

Figure 5 The sputtering sequence used to obtain wrinkle-free tantalum films. (a) Porous d.c. sputtered tantalum films. (b) (c) and (d) represent r.f. sputtering without magnetron, at a forward power of 400, 300 and 200 W respectively. (e) and (f) show wrinkle-free tantalum films deposited at 150 and 100 W respectively using r.f. magnetron sputtering.

ences, a large interfacial compressive stress developed upon cooling (Figs. 5b to d). This stress was sufficient to induce a large curvature in the polymer substrate which was relieved by the local detachment and buckling of the tantalum film over time.

The sputtering conditions were improved by superimposing a magnetic field during deposition which served to deflect the secondary electrons generated in the plasma away from the substrate (Magnetron conditions) [28]. The substrate temperature was further reduced by using low forward powers (100 to 150 W) and larger separations between substrate and target. At these lower deposition rates, it was necessary to reduce the residual gas pressure to 10^{-6} torr to prevent excessive oxidation. Unlike those films deposited at higher powers, no stress-induced curvature of the substrate was observed.

The ratio of polycrystalline β- to b c c-tantalum could be increased by decreasing the residual gas pressure prior to deposition. Neglecting defect broadening, the width of the [2 2 0] reflection was used to estimate a b c c crystal size of 5 nm (Fig. 6a) [29]. Both the [1 0 3] dark-field micrograph and the breadth of the electron diffraction rings from the β-tantalum film again revealed very small crystals of 2 to 4 nm (Figs. 6b, c). Anodization of both types of films provided the same amorphous Ta_2O_5 films (Fig. 6d). Islands of tantalum metal isolated close to the interface by fragmentation of the electrical path during the

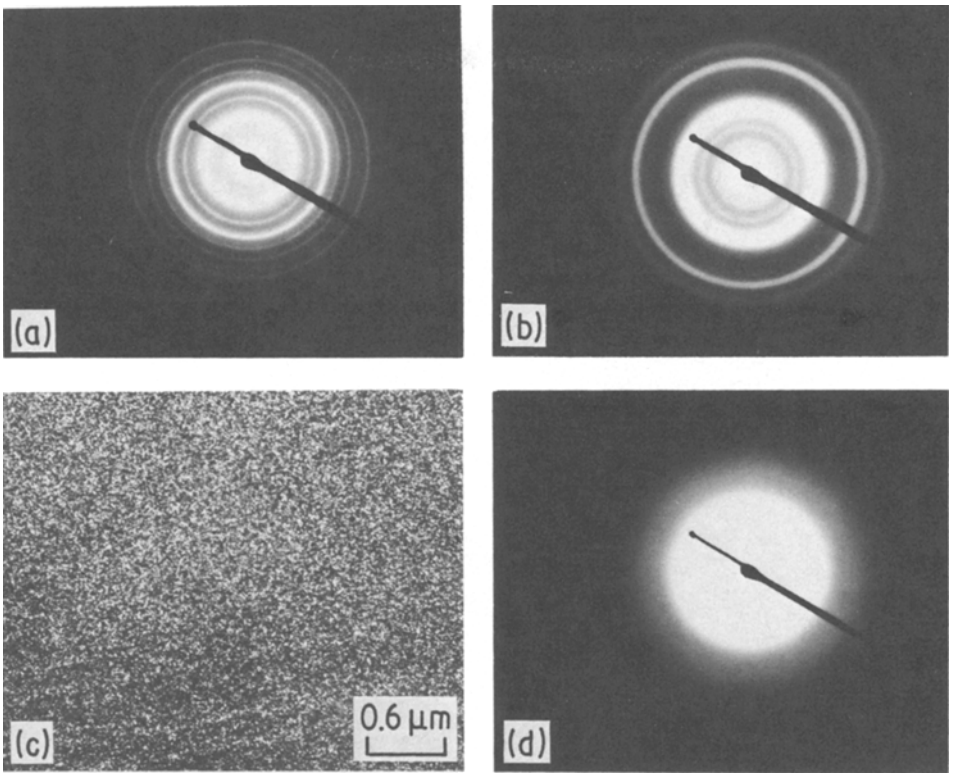

Figure 6 The crystal structure of the deposited tantalum films depends on the sputtering conditions. For high residual gas pressure (5×10^{-5} torr) b c c tantalum is deposited (a), while in better vacuum (4×10^{-7} torr) β-Ta is deposited (b). Both types of tantalum anodize completely into amorphous Ta_2O_5 (d). (c) Shows dark-field microscopy for β-Ta used to determine crystal size (5 nm in [1 0 3] direction).

final stages of anodization were expected but not seen even though XPS had detected a higher level of tantalum close to the substrate (Tables Ic, e).

Undeformed tantalum films were for the most part featureless (Fig. 7c), except for regions containing processing lines (Figs. 5e and f, horizontal lines) which were readily identified by their extent, which could reach 100 μm or more. Platinum–carbon shadow replicas of both the deformed and undeformed, uncoated polymer substrates clearly revealed the presence of the same processing lines (Fig. 8). Overlying Ta_2O_5 films also mimicked the substrate surface defects. An especially heavily scratched area is seen in Figs. 9a and b. Another morphology that was present in isolated areas of both the metal and oxide films on FEP substrates was a puckered structure (Figs. 9a and 7a) that could represent incipient detatchment from the substrate during deposition. The shadow effect appearing at the periphery of these bumps indicates that they formed at an early stage in the deposition process. In order to avoid confusion all deformed films were picked up in a known orientation on a microscope grid with a direction marker. Randomly oriented scratches could thus be identified.

Metallic tantalum films deformed to 5 and 10% tensile strain on the polymer substrates, regardless of the film thickness in the 30 to 60 nm range, plastically deformed by coarse slip bands (Figs. 7b, d). More finely dispersed slip bands as are sometimes seen in ductile amorphous polymers [30] could not be readily observed. As expected, these coarse bands grew along the directions of maximum resolved shear stress at 45° to the tensile axis (Fig. 7b, arrows a and b). The two slip lines that intersect shear each other, creating a jog at their intersection (arrow c). The shear deformation of the coarse bands is quite large as can be seen by the cracks induced within. Fig. 7d shows several bands containing considerably less deformation, that is a general feature of tantalum films deformed on Kapton substrates. Whether this morphology is related to a difference in

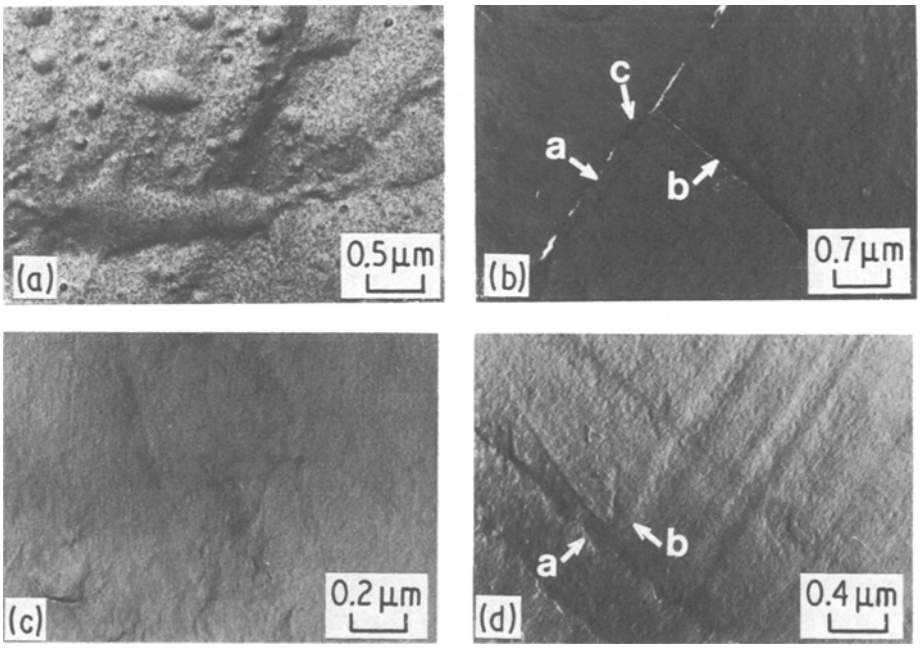

Figure 7 The morphological features of deposited tantalum on FEP and Kapton. (a) and (b) show Ta/FEP at 0% and 10% tensile deformation. (b) Shows clearly that Ta/FEP is directly deformed by slip bands where arrows a and b point to slip lines intersecting at 90°, shearing each other and forming a jog at arrow c. (c) Represents 0% deformation of Ta/Kapton, while (d) shows similar behaviour to Ta/FEP when it is deformed to 10% strain. The stress axis is along the horizontal direction, crystal structure is a mixture of β- and b c c-Ta. Film thickness is 80 nm.

adhesion or crystal morphology for tantalum films on the two substrates is unknown.

All anodized samples showed considerable ductility up to 10% elongation. For example, arrows a and b in Fig. 9b indicate shear bands formed in an amorphous Ta_2O_5 film deformed on FEP. The large deformation present in this region does give rise to a crack (arrow c). Localized deformation of this type was much more difficult to observe in films anodized on Kapton. However, in the vicinity of substrate surface defects shear bands could be observed (Fig. 9d). In cases where the oxide film had detached from the substrate over large areas, equally spaced cracks oriented perpendicular to the applied tensile strain were observed. This loss of adhesion was not noted at tensile strains less than or equal to 5%.

4. Discussion

At this point one is left to attempt an explanation of the deformation mechanism of both the tantalum metal and its amorphous oxide. Unfortunately, no one model explaining the ductility of amorphous materials is agreed upon. In either the sputter-deposited tantalum films, becuase of a very small crystal size, or in amorphous glassy Ta_2O_5, it would be difficult to postulate a dislocation mechanism consistent with a geometrically meaningful Burgers vector. However, some investigators have used the more general concept of a Volterra dislocation to explain the slip lines that have been observed in metallic glasses [31–33]. Argon [34] has been relatively successful in modelling the temperature dependency of the yield stress of amorphous polymer glasses by identifying a rather general dislocation concept with a double kink in a bundle of polymer chains. However, the strain softening which is necessary for the development of localized micro shearbands is still not explained by a molecular mechanism.

The development of any concept of strain localization in a glass depends upon the existence of heterogeneities in packing. One might imagine that if the heterogeneities were very finely dispersed with a rather narrow distribution in packing density then a rather uniform shear deformation might result. Young and Smith [35] have postulated that amorphous Ta_2O_5 consists of small densely packed regions that can move relatively easily in a more mobile matrix in which the

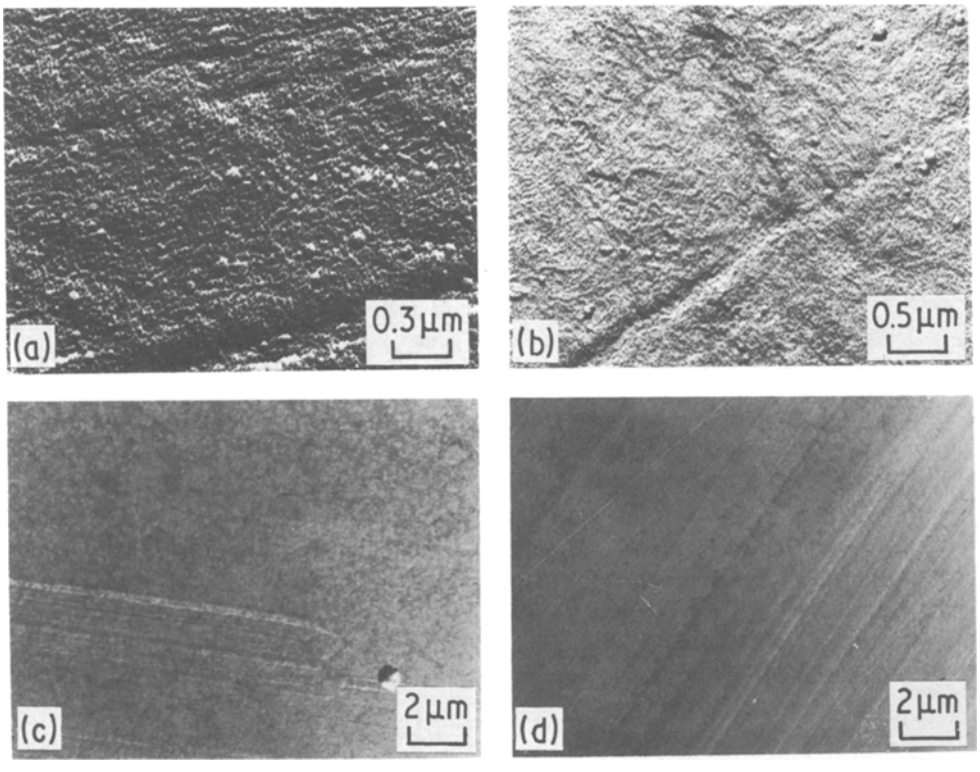

Figure 8 Carbon–platinum replicas of the polymer substrates FEP (a, b) and Kapton (c, d). Each substrate was deformed up to 10% strain [(b) and (d) for FEP and Kapton, respectively]. Note that both 0% and 10% show processing traces.

rigid three-dimensional angle constraints, typical of a ceramic structure, are removed. Young and Smith did not define these structures precisely but referred to the work of Roth *et al.* [36, 37] who studied the structure of semi-amorphous Ta_2O_5 produced by thermal treatment of an amorphous oxide. Interestingly, they postulated that this structure consisted of chains of pentagonal bipyramids with oxygen ions at the corners and tantalum ions in the centre. These chains are of various lengths and are capable of folding back upon themselves. One immediately calls to mind the facile interchain slip that occurs in organic polymers by fold pull-out between two adjacent segments of the same chain [38].

If such a deformation mechanism exists in oxides of tantalum, one might expect a distinct sub-T_g relaxation having a noticeable strain dependency. Small molecules such as water or polar organic molecules should have a significant effect on the interblock (or interchain) movement, which should be apparent in the dynamic mechanical spectrum or the stress–strain behaviour. Our further investigations into the mechanism of deformation of these oxides will follow this approach. At this juncture it is appropriate to mention that the oxygen excess that was detected by XPS in our Ta_2O_5 films, if it were strongly bound water, would certainly have an effect on the mechanical properties of the film. It is hoped to eliminate this factor by looking at directly sputter-coated Ta_2O_5. Finally, as mentioned above, the FEP is quite sensitive to the argon plasma. Conceivably fluorocarbon degradation products could have increased the ductility of both the metal and oxide films. However, experiments with the more stable polyimide film certainly provide strong evidence that both the very fine grained metal film and the oxide possess inherent ductility.

Acknowledgements

The authors would like to thank IBM for their financial support of this work and Dr Viswam Puligandla for his interest and helpful suggestions. Professor J. Sivertson is also acknowledged for his

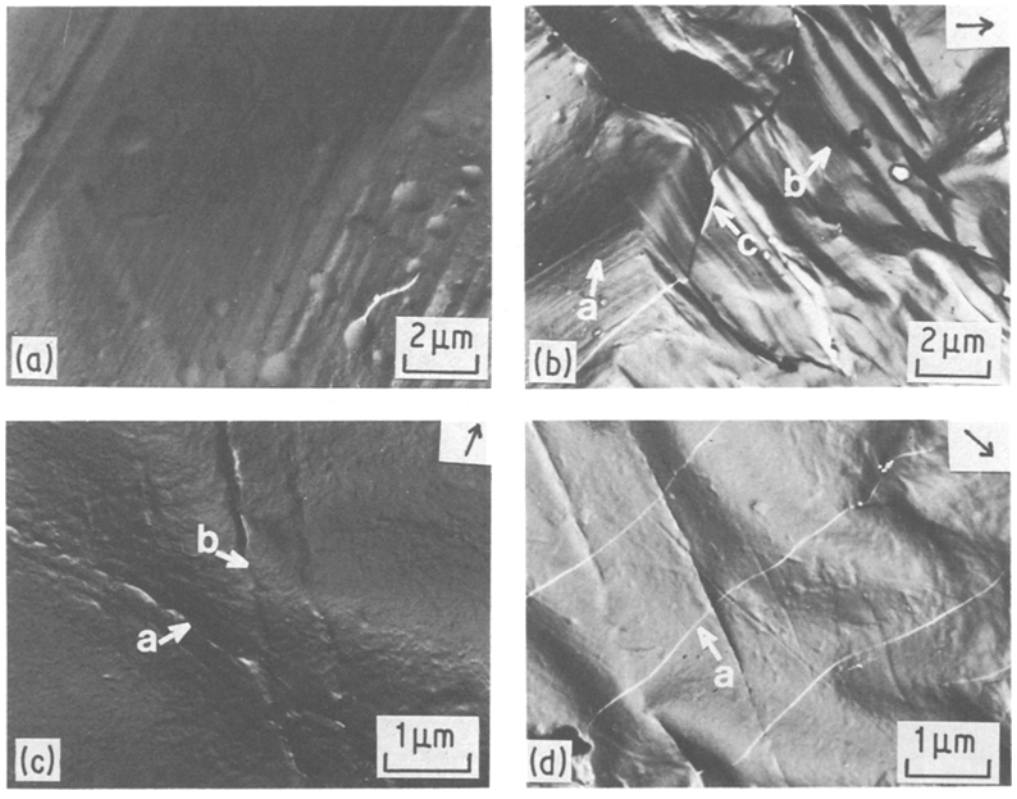

Figure 9 The deformation features of amorphous Ta_2O_5 films on FEP and Kapton when mechanically deformed under tension up to 10% strain. (a) and (b) show Ta_2O_5/FEP at 0% and 10% strain. Arrows a and b in Fig. 9b point to heavily plastically deformed regions while arrow c points to minor cracks. (c) Shows similar behaviour of Ta_2O_5/Kapton where deformed to 10% strain. (d) shows equally spaced cracks which are often observed. Original tantalum films have β-phase crystal structures and were 40 nm thick. The stress direction is indicated by the arrow in the upper right-hand corner of each figure.

many helpful discussions. The assistance of the NSF Regional Surface Science facility in obtaining the XPS results and Professor Bill Robbins for his guidance in the sputter-deposition part of the work are also gratefully acknowledged.

References

1. Y. H. CHOO and O. F. DEVEREUX, *J. Electrochem. Soc.* **123** (1976) 1868.
2. D. H. BRADHURST and J. S. L. LEACH, *ibid.* **113** (1966) 1245.
3. J. S. L. LEACH and P. NEUFELD, *Proc. Brit. Ceram. Soc.* **6** (1966) 49.
4. *Idem, Corros. Sci.* 9 (1969) 225.
5. N. J. COCHRANE and R. J. BLOCK, *J. Electrochem. Soc.* **117** (1970) 225.
6. P. MEHDIZADEH and R. J. BLOCK, *ibid.* **119** (1972) 1091.
7. C. EDELEAUU and T. J. LAW, *Phil. Mag.* 7 (1962) 573.
8. J. C. GROSSKREUTZ, *J. Electrochem. Soc.* **116** (1969) 1232.
9. *Idem, ibid.* **117** (1970) 940.
10. S. F. BUBAR and D. A. VERMILYEA, *ibid.* **11** (1966) 892.
11. D. ELIEZER and D. G. BRANDON, *Thin Solid Films* **12** (1972) 319.
12. M. PROPP and L. YOUNG, *J. Electrochem. Soc.* **126** (1979) 624.
13. L. YOUNG, "Anodic Oxide Films" (Academic Press, London, 1961) p. 69.
14. V. K. SETHI and R. GIBALA, *Thin Solid Films* **39** (1976) 79.
15. *Idem, Acta Metall.* **25** (1977) 332.
16. *Idem, Scripta Metall.* 9 (1975) 527.
17. *Idem*, in Proceedings of the 2nd International Conference on Mechanical Behaviour of Materials (American Society for Metals, Cleveland, OH, 1976) p. 73.
18. F. T. SISCO and E. EPREMIUAN (eds) "Columbium and Tantalum" (Wiley, New York, 1963).
19. H. K. YASUDA, paper presented at US Army Research Office Working Group Meeting on Protective Materials, Newport, RI, October 1982.
20. M. READ and C. ALTMAN, *Appl. Phys. Lett.* 7 (1965) 51.
21. R. BERRY, P. HALL and M. HARRIS, "Thin Film Technology" (Van Nostrand, New Jersey, 1968).

22. H. J. SCHWETZE, H. EHLBECH and G. DOERBECK, Transcriptions of the 10th National Vacuum Symposium (Macmillan Co., New York, 1963) p. 434.
23. W. D. WESTWOOD, *Thin Solid Films* **15** (1973) 15.
24. W. D. WESTWOOD and R. BOYNTON, *J. Appl. Phys.* **43** (1972) 2691.
25. L. G. FEINSTEIN and R. D. HUTTEMANN, *Thin Solid Films* **12** (1972) S47.
26. *Idem, ibid.* **16** (1973) 29.
27. L. ECKERTOVA, "Physics of Thin Films" (Plenum Press, New York, 1977).
28. L. MAISSEL, in "Handbook of Thin Films Technology", edited by L. Maissel and R. Glancy (McGraw-Hill Co., New York, 1970).
29. G. THOMAS and M. GORINGE, "Transmission Electron Olicroscopy of Materials", (John Wiley and Sons, New York, 1979).
30. S. T. WELLINGHOFF, E. BAER and J. L. KOENIG, *J. Polym. Sci. Phys.* **15** (11) (1977) 1913.
31. J. C. M. LI, in "Frontiers in Materials Science", edited by L. Muir and C. Stein (Marcel Dekker, Inc., New York, 1976) p. 527.
32. J. J. GILMAN, "Dislocation Dynamics", edited by A. R. Rosenfield *et al.* (McGraw-Hill, New York, 1968).
33. J. C. LI, "Metallic Glasses" (American Society for Metals, Metals Park, OH, 1976) p. 224.
34. A. S. ARGON, *Phil. Mag.* **28** (1973) 839.
35. L. YOUNG and D. J. SMITH, *J. Electrochem. Soc.* **126** (1979) 765.
36. R. S. ROTH and N. C. STEPHEN, "Chemistry of Extended Defects in Solids", (North Holland, Amsterdam, 1976) p. 167.
37. N. C. STEPHEN and R. S. ROTH, *Acta Crystallogr. Sect. B* **27** (1971) 1037.
38. J. M. SHULTZ, "Polymer Materials Science" (Prentice Hall, Englewood Cliffs, NJ, 1974).

Received 29 December 1983
and accepted 18 January 1984